

Floxuridine Oligomers Activated under Hypoxic Environment

Kunihiko Morihiko, Takuro Ishinabe, Masako Takatsu, Hiraki Osumi, Tsuyoshi Osawa, and Akimitsu Okamoto*



Cite This: *J. Am. Chem. Soc.* 2021, 143, 3340–3347



Read Online

ACCESS |



Metrics & More

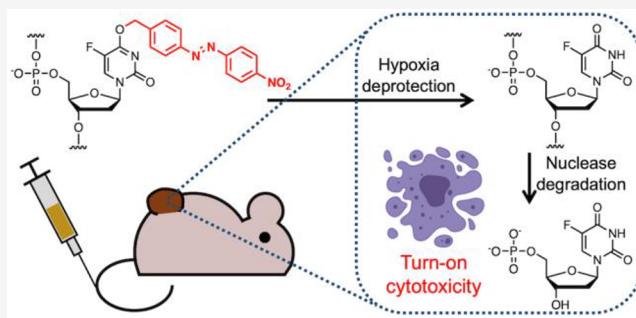


Article Recommendations



Supporting Information

ABSTRACT: Floxuridine oligomers are anticancer oligonucleotide drugs composed of a number of floxuridine residues. They show enhanced cytotoxicity per floxuridine monomer because the nuclease degradation of floxuridine oligomers directly releases highly active floxuridine monophosphate in cells. However, their clinical use is limited by the low selectivity against cancer cells. To address this limitation, we herein report floxuridine oligomer prodrugs that are active under hypoxia conditions, which is one of the distinguishing features of the microenvironment of all solid tumors. We designed and synthesized two types of floxuridine oligomer prodrugs that possess hypoxia-responsive moieties on nucleobases. The floxuridine oligomer prodrugs showed lower cytotoxicity under normoxia conditions ($O_2 = 20\%$), while the parent floxuridine oligomer showed similar anticancer effects under hypoxia conditions ($O_2 = 1\%$). The floxuridine oligomer prodrug enabled tumor growth suppression in live mice. This would be the first example demonstrating the conditional control of the medicinal efficacy of oligomerized nucleoside anticancer drugs.



INTRODUCTION

Chemotherapy is a fundamental treatment of cancer as well as surgery and radiation therapy. Fluoropyrimidines are traditional antimetabolites that are widely applied for the chemotherapy treatment of various solid tumors.¹ The compound 2'-deoxy-5-fluorouridine (floxuridine) is a clinically used fluoropyrimidine drug that was approved by the US FDA in 1970 under the brand name FUDR.² Floxuridine undergoes catabolism to form 5-fluorouracil, mediated by DNA glycosylases in the blood, and interferes with DNA and RNA synthesis. Floxuridine is also intracellularly monophosphorylated at its 5'-hydroxyl group by thymidine kinase and causes the inhibition of thymidylate synthetase, leading to thymineless cell death. Although floxuridine and its derivatives have effective anticancer activity, the systemic adverse effects, including bone marrow suppression, diarrhea, and stomach pain, need to be reduced to prevent therapy discontinuation.² These issues stem from their low tumor selectivity; hence, designing an anticancer agent that is selective for killing tumor cells would enable significant progress to be made in cancer chemotherapy.

To improve the tumor selectivity of anticancer agents, prodrug strategies have been successfully applied.³ Prodrugs are masked derivatives of drug molecules that undergo enzymatic or chemical transformations to release the active parent drugs, which can exert the therapeutic activity. The cancer-specific microenvironment can be used as a trigger for selective prodrug activation, and hypoxia is a distinguishing feature of solid tumors wherein the median oxygen

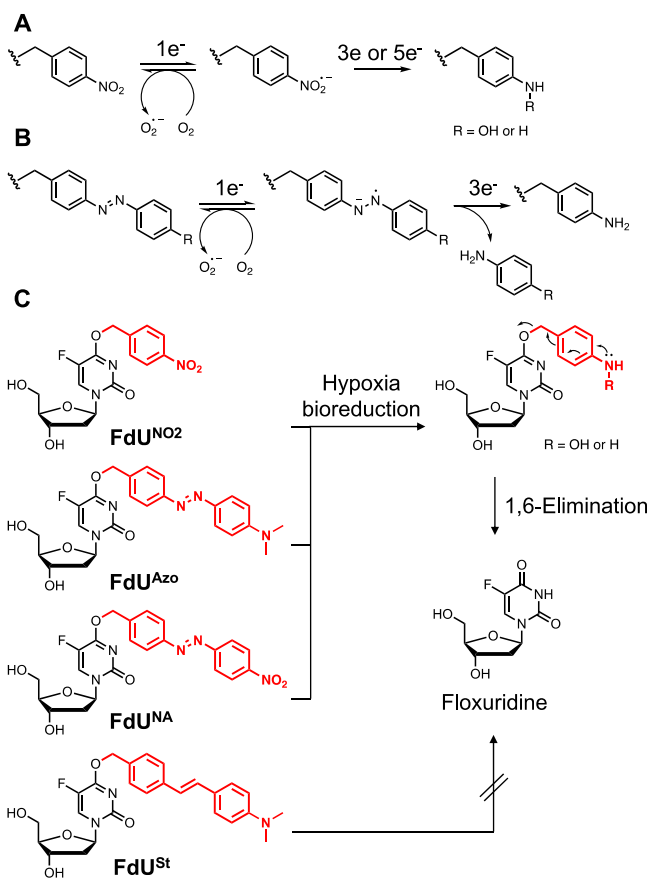
concentration is around 4%.⁴ Hence, hypoxia-mediated activation of anticancer prodrugs would contribute to the selective treatment of tumors and minimization of the adverse events. Tanabe and co-workers demonstrated the hypoxia-mediated activation of floxuridine prodrug bearing an indolequinone moiety, which is a substrate of reductases.⁵ Nitro and azo groups are also known to be reduced by some reductases in cells and work as hypoxia-sensitive moieties.⁶ The one-electron reduction of nitro and azo groups generates the radical anion, which can be reoxidized by oxygen under normoxia conditions (Scheme 1A,B). Meanwhile, under hypoxia conditions, the reoxidation is very slow and both moieties are reduced to amino groups. These hypoxia-sensitive moieties have been used to temporarily deactivate not only anticancer agents but also tumor imaging probes.⁶ In this study, we install azo and/or nitro functionality on the nucleobase of floxuridine and realize the hypoxia-selective inhibition of cancer cell proliferation. Further application includes the hypoxia-induced activation of floxuridine oligomers. This approach represents the first time oligomerized nucleoside anticancer drugs have been conditionally controlled in vitro and in vivo.

Received: October 9, 2020

Published: March 2, 2021



Scheme 1. Reduction Mechanisms of (A) Nitro and (B) Azo Functionality and (C) Hypoxia-Activated Floxuridine Prodrugs

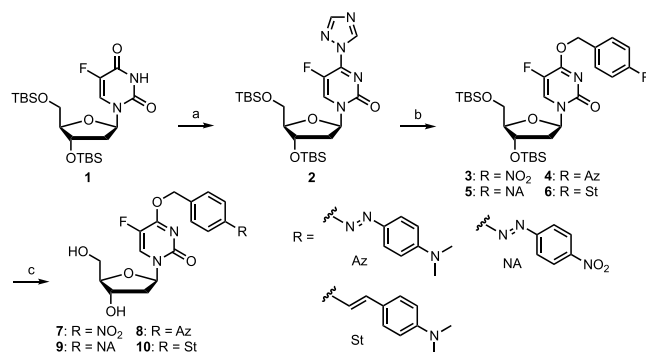


RESULTS AND DISCUSSION

We designed three types of caged floxuridine monomers, **FdU^{NO2}**, **FdU^{Azo}**, and **FdU^{NA}**, bearing a nitrobenzyl group, 4-(dimethylamino)azobenzyl group, and 4-nitroazobenzyl group, respectively (Scheme 1C). These hypoxia-sensitive moieties were installed on the 4-oxygen atom of floxuridine because the hydrogen-bonding interactions between thymidine kinase with the carbonyl oxygen in the 4-position are crucial for 5'-phosphorylation. **FdU^{NO2}** and **FdU^{Azo}** are directly reduced to the hydroxyl amine or aniline intermediate, and a subsequent 1,6-elimination gives floxuridine.⁸ In contrast, **FdU^{NA}** requires a two-phased reduction; the nitro group should be reduced first because the 4-nitroazobenzyl moiety is not a substrate of azoreductases.⁹ After the reduction of the nitro group, the azo moiety of **FdU^{NA}** is reduced to give the aniline intermediate. We can conclude that **FdU^{NO2}**, **FdU^{Azo}**, and **FdU^{NA}** require at most 6, 4, and 10 electrons, respectively, for the complete bioreduction to release floxuridine. **FdUSt** was considered a hypoxia-insensitive compound because of its C=C bond instead of azo functionality.

The synthetic details for each floxuridine prodrug are summarized in Scheme 2. In short, hypoxia-responsive and -unresponsive moieties were introduced by S_NAr reactions between O4-triazolyl-floxuridine analogue **2**¹⁰ and the corresponding benzyl alcohol. With the caged floxuridine monomers **7–10** in hand, we used high-performance liquid chromatography (HPLC) to measure the reactivity of each floxuridine prodrug against sodium dithionite ($Na_2S_2O_4$) as a

Scheme 2. Synthesis of Floxuridine Prodrugs^a



^aReagents and conditions: (a) 1,2,4-triazole, $POCl_3$, Et_3N , 0 °C to rt, 16 h, 88%; (b) 4-nitrobenzyl alcohol, DBU, MeCN, rt, 1.5 h, 92% (**3**); 4-[(4-dimethylaminophenyl)azo]benzyl alcohol, DBU, MeCN, 2 h, 78% (**4**); 4-[(4-nitrophenyl)azo]benzyl alcohol, DBU, MeCN, rt, 1.5 h, 24% (**5**); 4-[2-(4-dimethylaminophenyl)ethynyl]benzyl alcohol, DBU, MeCN, rt, 3 h, 61% (**6**); (c) TBAF, THF, rt, 8 h, 86% (**7**); TBAF, THF, rt, 2 h, quant. (**8**); TBAF, THF, rt, 4 h, 65% (**9**); TBAF, THF, rt, 4 h, 89% (**10**).

reducing agent (Figure S1).^{11–13} Due to the excess amount of $Na_2S_2O_4$, all caged monomers were reduced to floxuridine within 1 h, indicating that the designed compounds have excellent sensitivity toward reducing environments. We confirmed that **FdUSt**, which has a C=C bond instead of a N=N bond in **FdU^{Azo}**, did not react with $Na_2S_2O_4$. In contrast, floxuridine prodrugs did not react with biologically relevant reducing agent glutathione (GSH) and under weakly acidic conditions (pH 5.5), which are other unique characteristics of the microenvironment of tumors (Figure S1), indicating that the decaging reaction of nitro and azo functionality is hypoxia-selective. To further study the bioreduction of floxuridine prodrugs, **FdU^{NO2}**, **FdU^{Azo}**, and **FdU^{NA}** were incubated with rat liver microsomes and NADPH at 37 °C in argon-bubbled media (in vitro conditions that mimic those of hypoxia).^{14–20} As shown in Figure 1A, the amount of **FdU^{Azo}** and **FdU^{NA}** decreased under hypoxia-simulating conditions, whereas no consumption was observed in argon-unbubbled media. In contrast, **FdU^{NO2}** was not reduced under either normoxic- or hypoxia-mimicking conditions, indicating that **FdU^{NO2}** is more tolerant toward bioreduction than **FdU^{Azo}** and **FdU^{NA}**. Although rat liver microsomes do not completely reproduce the reductive environment in human cancer cells, the slow activation of 4-nitrobenzyl-modified fluorescent proven by them was reported.²¹ It is suggested that 4-nitrobenzyl moiety in small molecules is not a good substrate of rat liver microsomes. However, we cannot conclude that **FdU^{NO2}** does not work as a hypoxia-prodrug because there are many types of reductases in human cells such as methionine synthase reductase,²² NADPH-dependent diflavin oxidoreductase 1,²³ and nitric oxide synthase,²⁴ and their intracellular concentrations and localizations are complicated.

Hypoxic conditions make cancer cells more tolerant toward anticancer drugs by slowing the cell proliferation rate and inhibiting the cell death induced by p53. Moreover, the α -subunit of hypoxia-inducible factor-1 (HIF-1 α) protects cancer cells from drug-induced senescence.²⁵ Hence, we first checked the sensitivity of various human cancer cell lines against floxuridine under hypoxic conditions using a cell viability assay

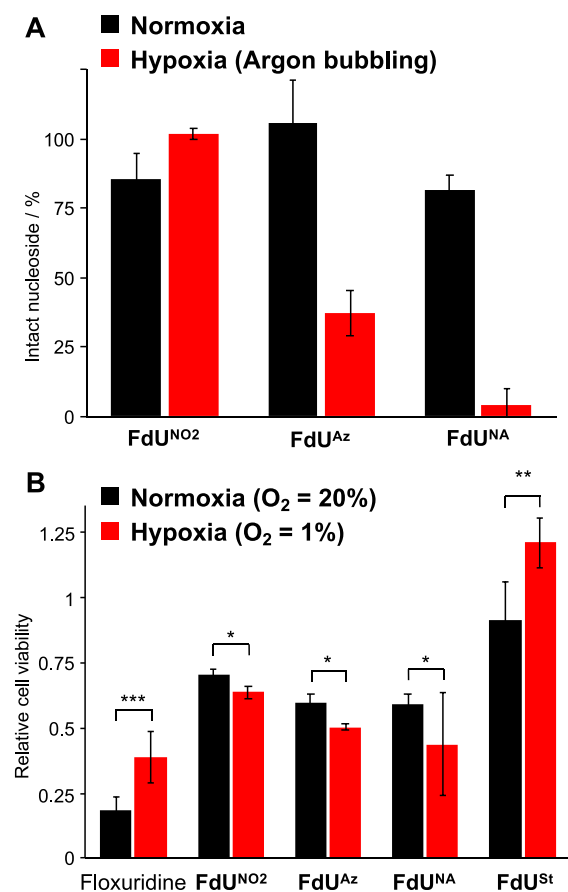


Figure 1. Hypoxia-induced activation of floxuridine monomer prodrugs. (A) Reduction of floxuridine monomer prodrugs by rat microsomes/NADPH for 1 h in argon-bubbled media. (B) Effects of floxuridine monomer prodrugs (1 μ M) on the viability of A549 cells under normoxia (O₂ = 20%) and hypoxia conditions (O₂ = 1%). Six independent experiments were averaged, and the error bars represent standard deviations. * $p \leq 0.05$, ** $p \leq 0.01$, and *** $p \leq 0.001$ by an unpaired Student's t test.

(Figure S2). Floxuridine was added to human lung cancer A549 cells, cervical cancer HeLa cells, fibrosarcoma HT1080, and colon cancer HCT116 and SW480 cells and incubated under normoxia (O₂ = 20%) or hypoxia (O₂ = 1%) conditions at 37 °C for 72 h using a hypoxic culture kit. Among the cancer cell lines we tested, A549 cells were the most sensitive to floxuridine under hypoxia, and therefore, we decided to use them in subsequent in vitro and in vivo experiments.

FdU^{Azo}, FdU^{NA}, and FdU^{NO2} were added to A549 cells at 1 μ M, and cell viability assays were conducted (Figure 1B). Importantly, floxuridine was less cytotoxic under hypoxia (O₂ = 1%) than under normoxia (O₂ = 20%) conditions, while all the prodrugs showed a higher cytotoxicity under hypoxia than under normoxia conditions. The smaller hypoxia-induced activation of FdU^{NO2} compared with FdU^{Azo} and FdU^{NA} may be explained by the in vitro experimental results that showed that FdU^{NO2} was more resistant to bioreductive conditions (Figure 1A). We confirmed that negative control FdUSt did not show cytotoxicity under either normoxic or hypoxic conditions because the C=C bond in FdUSt is nonbiodegradable. The concentration-dependent anticancer activity of each prodrug was also examined (Figure S3). To evaluate the hypoxia selectivity of each floxuridine prodrug more clearly, the cell viability at 1 μ M drug concentration was

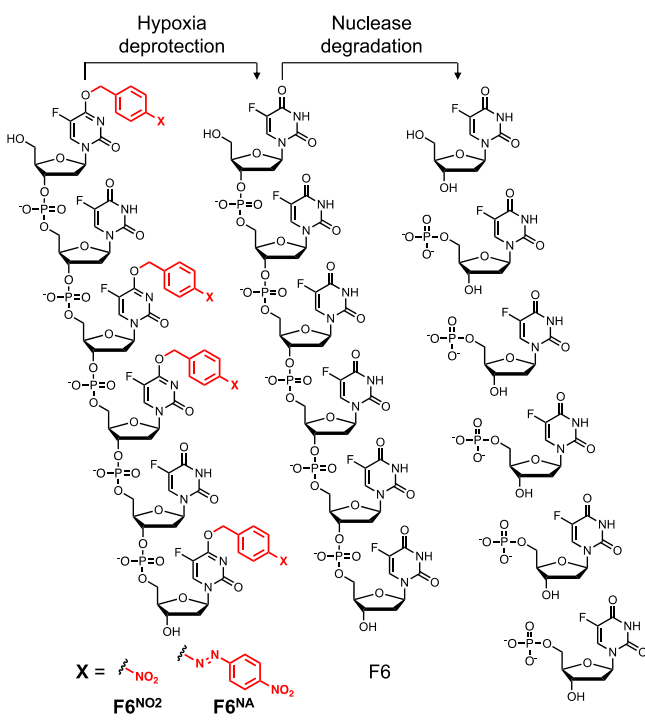
normalized relative to floxuridine. FdU^{NO2}, FdU^{Azo}, and FdU^{NA} showed much less cytotoxicity than floxuridine under normoxia conditions (3.8, 3.2, and 3.2 times, respectively), while they showed a similar cell viability as that of floxuridine under hypoxia conditions (1.6, 1.3, and 1.1 times, respectively). Together, the anticancer activity of our designed floxuridine prodrugs with nitro and/or azo functionality was turned on through hypoxia-mediated deprotection in human cancer cells. We confirmed that a negligible hypoxia activation of prodrugs was observed in HCT116 cells as expected (Figure S4).

Recently, floxuridine has been employed to construct floxuridine oligomers, which release highly cytotoxic floxuridine monophosphates and inhibit cell proliferation. Floxuridine oligomers show a greater cytotoxicity to human cancer cells per residue than monomeric floxuridine.²⁶ The enhancement in the cytotoxicity of floxuridine oligomers is attributed to a more efficient metabolism to the monophosphate than the floxuridine monomer.²⁷ Their effective delivery to tumors has been achieved using programmable DNA self-assembly,^{28,29} and a recent application has demonstrated the use of combinatorial chemo and gene therapy to treat drug-resistant cancers.^{30,31} The results of cell viability assay of caged floxuridine monomers prompted us to employ FdU^{NO2}, FdU^{Azo}, and FdU^{NA} to construct hypoxia-activated floxuridine oligomers. An oligomeric floxuridine of 6-mer length (F6) was chosen as the active form of the prodrugs because of its synthetic simplicity and higher cytotoxicity per residue than monomeric floxuridine.²⁶ Moreover, better pharmacokinetics in the body can be expected with shorter oligomers.

We synthesized hypoxia-activated F6 using an automated DNA synthesizer by a standard phosphoramidite method (Figure S5). The synthetic details of each modified phosphoramidite are described in the Supporting Information. Caged floxuridine nucleotides were introduced into both the 5'- and 3'-ends to protect F6 from exonucleases, and two nucleotides at the center position were also replaced for protection from endonucleases. Unfortunately, FdU^{Azo} decomposed under the DNA synthesis conditions; hence, we obtained F6^{NO2} and F6^{NA}, which have four FdU^{NO2} and FdU^{NA} nucleotides in the sequence, respectively (Scheme 3). F6^{NO2} and F6^{NA} have nuclease resistance because the presence of unnatural nucleobases hampers nuclease access to the phosphodiester backbone,³² and these compounds show no cytotoxicity under normoxia conditions. In contrast, after reduction to the parent F6 under hypoxia conditions, multiple highly cytotoxic floxuridine monophosphates are released by nuclease degradation, inducing effective anticancer activity.

To confirm the fate of the modified floxuridine oligomers, F6, F6^{NO2}, and F6^{NA} were incubated at 37 °C in 10% fetal bovine serum (FBS), a blood product known to contain a variety of nucleases, and the mixtures were analyzed at several incubation time points by HPLC. Unmodified F6 was mostly degraded within 1 h, while almost all F6^{NO2} and F6^{NA} remained (Figure 2A). F6^{NA} showed a longer half-life than F6^{NO2}, probably because the larger caging groups more effectively prevented nuclease access to the phosphodiester backbone. We detected intact F6^{NA} even after 48 h of incubation. The half-lives of F6, F6^{NO2}, and F6^{NA} in 10% FBS were calculated to be 0.6, 3.4, and 15.3 h, respectively. This indicates that caging groups can enhance F6 retention in blood. Both F6^{NO2} and F6^{NA} showed a rapid response to Na₂S₂O₄ and generated parent F6 in accordance with the

Scheme 3. Chemical Structure and Hypoxia-Mediated Activation of Caged Floxuridine Oligomers F6^{NO2} and F6^{NA}



reductive property of the corresponding nucleoside (Figure S6). Overall, caged floxuridine oligomers F6^{NO2} and F6^{NA} have a high nuclease resistance and would not exert their cytotoxicity until hypoxia-mediated bioreduction occurs.

To evaluate the hypoxia-induced activation of floxuridine oligomers in living cells, F6, F6^{NO2}, and F6^{NA} were incubated with A549 cells under normoxia (O₂ = 20%) or hypoxia (O₂ = 1%) conditions and cell viability assays were conducted. F6^{NO2} and F6^{NA} showed a much lower cytotoxicity than F6 at 0.1 μM concentrations, indicating that the caging groups effectively masked the anticancer ability of the floxuridine oligomer F6 under normoxia conditions (Figure 2B). In contrast, in hypoxia environments, F6^{NO2} and F6^{NA} both showed anticancer effects similar to that of F6. A better activation of F6^{NO2} than its monomeric form might be explained by the previous study showing that nitro groups in oligonucleotides are efficiently reduced by reductases.^{33–35} Again, importantly, the parent F6 was less cytotoxic under hypoxia than under normoxia conditions, while the cytotoxicities of F6^{NO2} and F6^{NA} were the opposite. The clear recovery in the drug efficacy of F6^{NO2} and F6^{NA} validates our design of hypoxia-responsive groups that are reduced by reductases and generate the active form of F6 only in hypoxic cells. Indeed, F6^{NO2} and F6^{NA} were 3.9 and 3.3 times less toxic than F6 under normoxia conditions, respectively. Meanwhile, the difference in anticancer activity between F6 and both F6^{NA} and F6^{NO2} was negligible under hypoxia conditions (2.0 and 1.3 times less toxic than F6, respectively). The similar therapeutic effects as floxuridine monomer prodrugs were observed even if the drug concentrations were 1/10, proving the high therapeutic efficacy of oligomerized floxuridine prodrugs. The concentration-dependent anticancer activities of both oligomer prodrugs were confirmed (Figure S7). The above results demonstrate the ability to conditionally activate a highly toxic floxuridine oligomer on the basis of a nucleobase caging strategy.

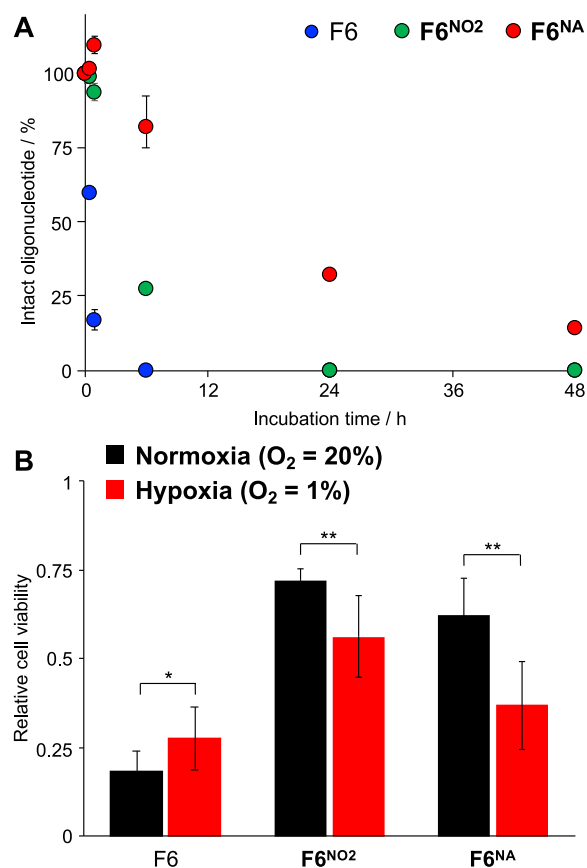


Figure 2. Properties of floxuridine oligomer prodrugs. (A) Nuclease degradation of floxuridine oligomer F6 and its prodrugs in 10% FBS within 48 h incubation time course. (B) Effects of floxuridine oligomer prodrugs (0.1 μM) on the viability of A549 cells under normoxia (O₂ = 20%) and hypoxia conditions (O₂ = 1%). Six independent experiments were averaged, and the error bars represent standard deviations. * $p \leq 0.05$ and ** $p \leq 0.01$ by an unpaired Student's t test.

To investigate whether our hypoxia-activated floxuridine is effective in vivo, we administered floxuridine oligomer prodrugs in A549-tumor-bearing BALB/cAJcl nude mice; solid tumors consist of hypoxic tumor microenvironments, which, in turn, were expected to activate the hypoxia-activated floxuridine within the tumor in vivo. We evaluated the therapeutic potential of F6^{NA}, which was the most potent F6 prodrug in vitro and in the cell viability experiments. A549 cells were implanted in BALB/cAJcl nude mice ($n = 6$ in each group) and grown until tumor sizes were around 100 mm³ before drug treatment. PBS, F6, or F6^{NA} was then intravenously administered (on days 0, 3, and 6). The changes in the tumor growth and the body weight were recorded during the treatment. As shown in Figure 3A–C, F6^{NA} was found to efficiently inhibit the tumor growth at the same levels as F6, approximately 2.5-fold reduction in tumor growth, suggesting that F6^{NA} recognized the hypoxic tumor microenvironment and was activated within the region. We also want to emphasize the reliability of F6^{NA} efficacy because there was little variance in tumor size of F6^{NA}-treated mice compared with those of F6-treated mice (Figure 3A,C). The changes of body weight in the F6^{NA}-treated group were similar to those of the PBS control group (Figure S8), suggesting the F6^{NA} has minor toxicity to the mice. We also measured the alanine

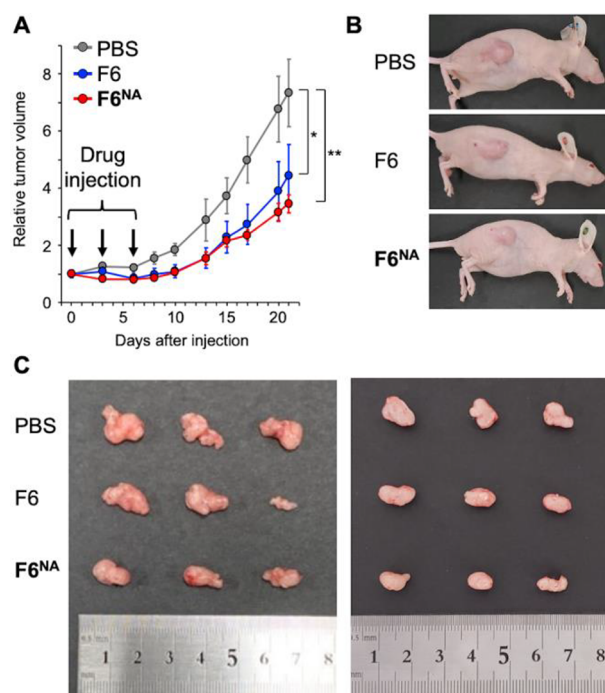


Figure 3. In vivo evaluation of F6^{NA} as an anticancer agent. (A) Tumor volumes of each group ($n = 6$). (B) Representative images of mice on day 21. (C) Photograph of tumors dissected from nude mice on day 21. Error bars represent standard errors. * $p \leq 0.05$ and ** $p \leq 0.01$ by an unpaired Student's t test.

aminotransaminase (ALT) levels to evaluate the detailed adverse effects because some synthetic oligonucleotides are known to have severe hepatotoxicity.³⁶ F6^{NA} did not result in elevated ALT levels compared to a positive control (Figure S9), which means the adverse effect of F6^{NA} is very low.

Taken together, these results indicate that F6^{NA} is a promising anticancer prodrug targeting hypoxic tumor micro-environments. Our approach enables the specific activation of oligomerized nucleoside drugs, which has attracted great attention as a new antitumor drug platform because of their higher therapeutic efficacy. Furthermore, we can propose a new hypoxia-responsive 4-nitroazobenzyl group, which shows excellent bioreductive properties compared to traditional caging groups. This can be applied to develop hypoxia-sensitive prodrugs based on not only nucleoside molecules but also other modalities including peptides. For developing future drug therapies, the molecular design of the oligomerized prodrugs can be adapted to other nucleic acid therapeutics, including antisense oligonucleotides (ASOs), small interfering RNAs (siRNAs), and aptamers.³⁷ On the contrary, the tumor suppression effect of our prodrug in mice was not so dramatic. Thus, our future work will include the optimization of the length of floxuridine oligomers and the pattern of nucleobase protections.

CONCLUSIONS

We have developed an oligomerized floxuridine that is activated in hypoxia environments by the installation of nitro and azo functionalities onto the 5-fluorouracil nucleobases. The introduction of hypoxia-responsive groups abolished the cytotoxicity of floxuridine oligomer in normoxia conditions ($O_2 = 20\%$) through the enhancement of nuclease resistance. In contrast, under hypoxia conditions ($O_2 = 1\%$), nitro and azo

functionalities were reduced by intracellular reductases into amino groups, generating highly cytotoxic floxuridine oligomer in situ. We also evaluated the anticancer activity of the floxuridine oligomer prodrug in vivo. Collectively, the results imply that our approach has great potential for an efficient targeted therapy of tumors.

EXPERIMENTAL SECTION

General. All chemicals were purchased from Sigma-Aldrich, Wako Chemicals, Tokyo Chemical Industry, and Glen Research. Reagents were used as received from commercial suppliers unless otherwise specified. Air- and/or moisture-sensitive experiments were carried out under a N_2 or Ar atmosphere. TLC was run on silica gel 60 F₂₅₄ aluminum sheets (Merck). Column chromatography was carried out with silica gel (Kanto Chemical; Silica Gel 60 (spherical), 63–210 μm) or reverse phase silica gel (Merck; LiChroprep RP-18, 40–63 μm). ^1H , ^{13}C , and ^{31}P NMR spectra were measured with an Avance 600 (Bruker Biospin), operating at 600, 150, and 240 MHz, respectively. Chemical shifts are reported in parts per million referenced to internal tetramethylsilane (0.00), residual CHCl_3 (7.26), methanol (3.31), or $\text{DMSO-}d_6$ (2.50) for ^1H NMR and chloroform- d (77.16), methanol- d_4 (49.00), or $\text{DMSO-}d_6$ (39.52) for ^{13}C NMR. Electrospray ionization mass (ESI-MS) spectrometry was recorded by a microTOF II-NAC (Bruker Daltonics). Matrix-assisted laser desorption ionization time-of-flight (MALDI-TOF) mass spectrometry was performed by a microflex-NAC (Bruker Daltonics). Modified oligonucleotides were synthesized on an NTS H-8 DNA/RNA synthesizer (Nihon Techno Service) and then purified by a HPLC system composed by GILSON and JASCO modules. The pH was measured by LAQUA F-72 (Horiba).

Synthesis of 2. To a solution of 1,2,4-triazole (4.33 g, 62.7 mmol) in MeCN (150 mL) were added POCl_3 (2.5 mL, 26.8 mmol) and Et_3N (10.2 mL, 73.2 mmol), and the mixture was stirred for 1 h in an ice bath. Then, compound **1**¹⁰ (1.87 g, 3.95 mmol) in MeCN (25 mL) was added, and the mixture was stirred for 16 h at room temperature. The reaction was quenched with saturated aqueous NaHCO_3 and evaporated. The mixture was extracted with DCM and applied to silica gel column (hexanes/ $\text{EtOAc} = 3/4$ (v/v)) to yield compound **2** as a white solid (1.83 g, 88%). ^1H NMR (600 MHz, CDCl_3): δ 9.25 (1H, s), 8.85 (1H, d, $J = 6$ Hz), 8.22 (1H, s), 6.22 (1H, s), 4.42 (1H, dd, $J = 12$ and 6 Hz), 4.06–4.02 (2H, m), 3.82 (1H, d, $J = 12$ Hz), 2.63–2.58 (1H, m), 2.25–2.21 (1H, m), 0.94 (9H, s), 0.89 (9H, s), 0.16–0.07 (12H, m). ^{13}C NMR (151 MHz, CDCl_3): δ 154.8, 154.6, 151.7, 148.9, 148.8, 145.4, 145.2, 144.3, 136.9, 135.2, 88.3, 88.2, 87.8, 87.7, 87.3, 69.8, 69.7, 61.7, 42.4, 25.9, 25.7, 18.5, 17.9, -4.1, -4.5, -4.9. ESI-MS calculated for $\text{C}_{23}\text{H}_{40}\text{FN}_5\text{O}_4\text{Si}_2$ m/z [$\text{M} + \text{Na}$]⁺: 548.2501; found 548.2504.

Synthesis of 3. To a solution of compound **2** (320 mg, 0.61 mmol) and 4-nitrobenzyl alcohol (100 mg, 0.65 mmol) in THF (6.2 mL) was added DBU (0.14 mL, 0.938 mmol), and the mixture was stirred at room temperature for 1.5 h. The mixture was evaporated and extracted with DCM and applied to silica gel column (hexanes/ $\text{EtOAc} = 2/1$ (v/v)) to yield compound **3** as a yellow solid (595 mg, 92%). ^1H NMR (600 MHz, CDCl_3): δ 8.35 (1H, d, $J = 6$ Hz), 7.59 (2H, d, $J = 6$ Hz), 6.18 (1H, s), 5.55 (2H, s), 4.36 (1H, d, $J = 6$ Hz), 3.96–3.91 (2H, m), 3.76 (1H, d, $J = 12$ Hz), 2.47–2.43 (1H, m), 2.11–2.07 (1H, m), 0.89–0.84 (18H, s), 0.10–0.03 (12H, s). ^{13}C NMR (151 MHz, $\text{DMSO-}d_6$): δ 161.9, 161.8, 153.4, 148.2, 142.6, 137.4, 135.8, 129.2, 128.6, 124.2, 124.1, 88.3, 87.5, 87.2, 87.1, 86.7, 70.6, 70.5, 67.9, 62.3, 26.3, 26.1, 18.8, 18.3, -3.8, -4.2, -4.6, -5.0. ESI-MS calculated for $\text{C}_{28}\text{H}_{44}\text{FN}_5\text{O}_7\text{Si}_2$ m/z [$\text{M} + \text{Na}$]⁺: 632.2600; found 632.2609.

Synthesis of 4. To a solution of compound **2** (736 mg, 1.03 mmol) and 4-[(4-dimethylaminophenyl)azo]benzyl alcohol (446 mg, 1.75 mmol) in MeCN (14 mL) was added DBU (0.46 mL, 3.08 mmol), and the mixture was stirred in ice bath for 5 min and then room temperature for overnight. The mixture was evaporated and extracted with DCM and applied to silica gel column (hexanes/ $\text{EtOAc} = 3/2$ (v/v)) to yield compound **4** as an orange solid (780 mg,

78%). ¹H NMR (600 MHz, CDCl₃): δ 8.32 (1H, d, *J* = 6 Hz), 7.88 (2H, d, *J* = 12 Hz), 7.85 (2H, d, *J* = 6 Hz), 7.56 (2H, d, *J* = 6 Hz), 6.76 (2H, d, *J* = 12 Hz), 6.25 (1H, s), 5.57 (1H, d, *J* = 12 Hz), 5.52 (1H, d, *J* = 12 Hz), 4.40 (1H, d, *J* = 6 Hz), 3.98 (1H, d, *J* = 12 Hz), 3.94 (1H, s), 3.79 (1H, d, *J* = 12 Hz), 3.10 (6H, s), 2.50–2.47 (1H, m), 2.17–2.12 (1H, m), 0.92 (9H, s), 0.88 (9H, s), 0.13–0.06 (12H, s). ¹³C NMR (151 MHz, CDCl₃): δ 161.9, 161.8, 153.2, 153.1, 152.4, 143.4, 137.2, 135.7, 135.6, 129.6, 129.4, 128.7, 128.5, 128.1, 127.9, 125.5, 125.4, 124.7, 124.5, 122.8, 122.7, 121.8, 111.32, 87.7(3), 87.6(6), 86.0, 70.0, 69.9, 61.8, 40.6, 39.8, 26.1, 25.9, 25.8, 25.7, 25.5, 18.4, 17.9, –5.2, –5.3, –5.9. ESI-MS calculated for C₃₆H₃₄FN₅O₃Si₂ *m/z* [M + Na]⁺: 734.3540; found 734.3548.

Synthesis of 5. To a solution of compound 2 (1.50 g, 2.86 mmol) and 4-[(4-nitrophenyl)azo]benzyl alcohol (868 mg, 3.38 mmol) in THF (29 mL) was added DBU (0.65 mL, 4.35 mmol), and the mixture was stirred at room temperature for 1.5 h. The mixture was evaporated and extracted with DCM and applied to silica gel column (hexanes/EtOAc = 3/1 to 2/1 to 1/1 (v/v)) to yield compound 5 as an orange solid (482 mg, 24%). ¹H NMR (600 MHz, CDCl₃): δ 8.31 (2H, d, *J* = 6 Hz), 8.29 (1H, d, *J* = 6 Hz), 7.97 (2H, d, *J* = 6 Hz), 7.91 (2H, d, *J* = 12 Hz), 7.57 (2H, d, *J* = 6 Hz), 6.19 (1H, d, *J* = 6 Hz), 5.53 (2H, t, *J* = 12 Hz), 4.34 (1H, t, *J* = 6 Hz), 3.93–3.88 (2H, m), 3.73 (1H, d, *J* = 12 Hz), 2.45–2.41 (1H, m), 2.09–2.05 (1H, m), 0.86 (9H, s), 0.82 (9H, s), 0.07–0.00 (12H, m). ¹³C NMR (151 MHz, CDCl₃): δ 162.2, 162.1, 156.0, 153.6, 152.6, 149.2, 139.8, 137.6, 136.0, 129.9, 129.6, 129.1, 128.8, 128.6, 125.1, 124.3, 123.7, 88.3, 70.7, 70.6, 68.8, 62.4, 26.3, 26.1, 25.9, 18.8, 18.3, –4.8, –4.9, –5.4. ESI-MS calculated for C₃₄H₄₈FN₅O₇Si₂ *m/z* [M + Na]⁺: 736.2968; found 736.2862.

Synthesis of 6. To a solution of compound 2 (228 mg, 0.380 mmol) in THF (9 mL) was added DBU (0.14 mL, 0.938 mmol), and the mixture was stirred at room temperature for 3 h. The mixture was evaporated and extracted with EtOAc and applied to silica gel column (hexanes/EtOAc = 3/1 (v/v)) to yield compound 6 as a yellow solid (188 mg, 61%). ¹H NMR (600 MHz, DMSO-*d*₆): δ 8.24 (1H, d, *J* = 6 Hz), 7.40 (2H, d, *J* = 6 Hz), 7.33 (4H, t, *J* = 12 Hz), 6.98 (1H, d, *J* = 18 Hz), 6.82 (1H, d, *J* = 12 Hz), 6.62 (2H, d, *J* = 6 Hz), 6.18 (1H, t, *J* = 6 Hz), 5.43 (1H, d, *J* = 12 Hz), 5.37 (1H, d, *J* = 12 Hz), 4.33 (1H, t, *J* = 6 Hz), 3.91–3.86 (1H, m), 3.71 (1H, d, *J* = 12 Hz), 2.88 (6H, s), 2.44–2.40 (1H, m), 2.09–2.05 (1H, m), 0.85 (9H, s), 0.82 (9H, s), 0.06–0.00 (12H, m). ¹³C NMR (151 MHz, DMSO-*d*₆): δ 162.4(3), 162.3(5), 153.7, 150.6, 139.1, 137.7, 136.1, 133.4, 130.0, 129.9, 129.8, 129.6, 129.4, 129.1, 129.0(6), 128.9(5), 128.5, 128.4, 128.2, 128.1, 129.0, 127.7, 127.0, 126.7, 126.3, 126.0, 125.9, 124.0, 112.8(0), 112.7(5), 88.2, 87.5, 87.4, 87.0, 86.9, 86.6, 86.4, 70.6, 70.5, 69.7, 62.3, 41.3, 41.0, 40.8, 40.7, 40.5, 40.4, 40.2, 18.8, 18.4, –4.8, –4.9, –5.5. ESI-MS calculated for C₃₆H₃₄FN₅O₃Si₂ *m/z* [M + Na]⁺: 732.3635; found 732.3663.

Synthesis of 7. To a solution of compound 3 (2.22 g, 3.65 mmol) in THF (37 mL) was added TBAF (1.0 M THF solution, 8.0 mL, 8.00 mmol), and the mixture was stirred at room temperature for 8 h. The mixture was evaporated, and H₂O was added. The liquid was filtered off, and the resultant solid was applied to silica gel column (MeOH/DCM = 22/1 (v/v)) to yield compound 7 as a white solid (1.20 g, 86%). ¹H NMR (600 MHz, DMSO-*d*₆): δ 8.68 (1H, d, *J* = 12 Hz), 8.38 (2H, d, *J* = 12 Hz), 7.84 (2H, d, *J* = 12 Hz), 6.18 (1H, t, *J* = 6 Hz), 5.68 (2H, s), 5.38 (1H, d, *J* = 6 Hz), 5.32 (1H, d, *J* = 6 Hz), 4.35 (1H, s), 3.95 (1H, s), 3.79–3.76 (1H, m), 3.72–3.69 (1H, m), 2.38–2.34 (1H, m), 2.20–2.16 (1H, m). ¹³C NMR (151 MHz, DMSO-*d*₆): δ 153.0, 148.1, 144.0, 135.6, 130.2, 129.2, 124.6, 88.7, 70.4, 70.3, 68.0. ESI-MS calculated for C₂₂H₂₀FN₅O₇ *m/z* [M + Na]⁺: 404.0870; found 404.0889.

Synthesis of 8. To a solution of compound 4 (780 mg, 1.61 mmol) in THF (11 mL) was added TBAF (1.0 M THF solution, 2.5 mL, 2.50 mmol), and the mixture was stirred at room temperature for 2 h. The mixture was evaporated and applied to a silica gel column (MeOH/EtOAc = 1/18 (v/v)) to yield compound 8 as an orange solid (596 mg, quant). ¹H NMR (600 MHz, DMSO-*d*₆): δ 8.60 (1H, d, *J* = 6 Hz), 7.83 (4H, d, *J* = 6 Hz), 7.62 (2H, d, *J* = 12 Hz), 6.82 (2H, d, *J* = 12 Hz), 6.13 (1H, s), 5.49 (2H, s), 5.35–5.29 (2H, m),

4.29 (1H, s), 3.89 (1H, s), 3.71 (2H, d, *J* = 12 Hz), 3.06 (6H, s), 2.31 (1H, t, *J* = 6 Hz), 2.12 (1H, dd, *J* = 12 and 6 Hz). ¹³C NMR (151 MHz, DMSO-*d*₆): δ 61.1, 161.0, 152.6, 152.4, 142.6, 136.6, 134.9, 129.9, 129.7, 129.3, 129.0, 128.9, 128.8, 125.5, 125.4, 125.0, 124.9, 124.6, 124.4, 122.5, 122.4, 122.1, 121.6, 121.5, 111.6, 87.8, 86.7, 85.7, 69.6, 69.5, 68.3. ESI-MS calculated for C₂₄H₂₆FN₅O₃ *m/z* [M + Na]⁺: 506.1810; found 506.1839.

Synthesis of 9. To a solution of compound 5 (1.46 g, 2.05 mmol) in THF (20 mL) was added AcOH (0.26 mL, 4.55 mmol) and TBAF (1.0 M THF solution, 4.6 mL, 4.60 mmol), and the mixture was stirred at room temperature for 4 h. The mixture was evaporated, and H₂O was added to the resulting orange solid. The liquid was filtered off, and then, the remaining solid was applied to a silica gel column (MeOH/DCM = 1/20 (v/v)) to yield compound 9 as an orange solid (645 mg, 65%). ¹H NMR (600 MHz, DMSO-*d*₆): δ 8.57 (1H, d, *J* = 6 Hz), 8.46 (2H, d, *J* = 6 Hz), 8.11 (2H, d, *J* = 12 Hz), 8.02 (2H, d, *J* = 6 Hz), 7.73 (2H, d, *J* = 6 Hz), 6.09 (1H, t, *J* = 6 Hz), 5.56 (2H, s), 5.29 (1H, d, *J* = 6 Hz), 5.22 (1H, t, *J* = 6 Hz), 4.25 (1H, s), 3.86 (1H, d, *J* = 6 Hz), 3.69–3.67 (1H, m), 3.61–3.59 (1H, m), 2.29–2.25 (1H, m), 2.11–2.07 (1H, m). ¹³C NMR (151 MHz, DMSO-*d*₆): δ 161.8, 161.7, 155.9, 153.1, 152.4, 149.4, 140.9, 137.2, 135.6, 130.5, 130.2, 129.5, 125.9, 124.4, 124.1, 123.8, 123.6, 88.7, 86.5, 70.4, 70.3, 68.6, 61.4. ESI-MS calculated for C₂₂H₂₀FN₅O₇ *m/z* [M + Na]⁺: 508.1239; found 508.1211.

Synthesis of 10. To a solution of compound 6 (53 mg, 74.7 μmol) in THF (1 mL) was added TBAF (1.0 M THF solution, 164 μL, 164 μmol), and the mixture was stirred at room temperature for 1 h. The mixture was evaporated and applied to a silica gel column (MeOH/EtOAc = 1/18 (v/v) and MeOH/DCM = 1/184 (v/v)) to yield compound 10 as a yellow solid (32 mg, 89%). ¹H NMR (600 MHz, DMSO-*d*₆): δ 8.36 (1H, d, *J* = 6 Hz), 7.47 (2H, d, *J* = 6 Hz), 7.42 (2H, d, *J* = 6 Hz), 7.26 (2H, d, *J* = 6 Hz), 7.09 (1H, d, *J* = 12 Hz), 6.94 (1H, d, *J* = 18 Hz), 6.71 (2H, d, *J* = 12 Hz), 6.19 (1H, t, *J* = 6 Hz), 5.30 (1H, s), 5.22 (1H, d, *J* = 6 Hz), 4.97 (2H, d, *J* = 6 Hz), 4.25 (1H, s), 3.80 (1H, s), 3.63–3.52 (2H, m), 2.92 (6H, s), 2.16 (2H, d, *J* = 6 Hz). ¹³C NMR (151 MHz, DMSO-*d*₆): δ 157.5, 157.3, 150.8, 149.9, 139.6, 138.0, 135.6, 129.4, 128.8, 127.9, 127.1, 126.1, 125.7, 113.1, 88.5, 70.8, 70.7. ESI-MS calculated for C₂₆H₂₈FN₃O₅ *m/z* [M + H]⁺: 482.2087; found 482.2089.

Hypoxia Activation with Rat Liver Microsomes *in Vitro*. The hypoxic condition was prepared by bubbling argon gas into the reaction solution (0.1 M potassium phosphate buffer, pH 7.4) for 30 min. Rat liver microsomes (140 μg/mL) purchased from BioIVT were preincubated at 37 °C for 5 min, and then, a 1 μM prodrug containing 1% DMSO as a cosolvent was added. As a cofactor for reductases, 100 μM nicotinamide adenine dinucleotide phosphate (NADPH) was added at 5 min.

Oligonucleotide Synthesis. All modified oligonucleotides were synthesized using a standard DNA synthesis method. Each phosphoramidite was dissolved in dry acetonitrile and filtrated to prepare a 0.1 M solution. Each phosphoramidite solution was reacted on a DNA synthesizer with 0.25 or 0.5 M 5-ethylthio-1H-tetrazole solution as an activator for 9 min. Glen UnySupport FC (Glen Research) was used for the synthesis. For the deprotection of DMTr protecting group, 3% DCA solution was used instead of 3% TCA solution. For every sequence, a 5'-end DMTr protecting group was eliminated on the synthesizer. Synthesized DNA was cleaved from the support by 28% ammonium solution at room temperature for 5 min. Immediately after the cleavage, the solution was purified through NAP-10 or -5 columns (GE Healthcare) to eliminate ammonium solution. All the products were purified by a reverse-phased HPLC.

Cell Viability Assay. The monolayer cell culture was trypsinized and counted. To each well of the 96-well plate was 180 μL of the diluted cell suspension (10 000 cells/mL). After 24 h, when a partial monolayer was formed, the medium in each well was removed by aspiration and 180 μL of fresh medium with different compound concentrations (0.001, 0.01, 0.1, or 1.0 μM) was added to each well. An hypoxia environment (O₂ concentration of 1%) was generated with an nBIONIX (Sugiyama-Gen). After 72 h, 20 μL of Prestoblu (Invitrogen) was added to each well, and the plate was incubated for 1

h. The fluorescence of each well was measured spectrophotometrically in a multiwell Cytation 5 plate reader (BioTek Instruments) at a wavelength of 590 nm, excited by a wavelength of 560 nm. The relative viability was calculated according to the following formula with the fluorescence intensity obtained:

$$\text{relative cell viability (x } \mu\text{M)} = \frac{\text{average (x } \mu\text{M)} - \text{average (DMEM)}}{\text{average (0 } \mu\text{M)} - \text{average (DMEM)}}$$

Nuclease Degradation Assay. In a 0.6 mL plastic tube, 72 μL of 10% FBS in $1 \times$ DMEM (+Pe/St), 5 μL of 100 μM Rhodamine B dissolved in MQ, and 3 μL of 10 μM F6 derivatives in MQ were mixed. The mixture was reacted for several hours at 37 $^{\circ}\text{C}$. The reaction mixture was filtered and analyzed by reverse phased HPLC. The relative peak area of the F6 derivatives was calculated by the dividing peak area of the F6 derivatives (260 nm) by that of Rhodamine B (550 nm).

In Vivo Studies. F6 (10 nmol) and F6^{NA} (10 nmol) were dissolved in 100 μL of PBS solution to a final concentration of 100 μM . Seven week old BALB/cA_Jcl nude mice (purchased from CLEA) were subcutaneously implanted with tumors by the injection of A549 cells. Nine nude mice were randomly assigned to three groups. After the implanted tumors were grown to about 100 mm³, drug injections (intravenous) were performed over a period of 3 days, and the length and width of the tumors were recorded. The tumor volume was calculated as $V = (a \cdot b^2)/2$, where V , a , and b indicate the tumor volume, length of tumor, and width of tumor, respectively. The experiments were repeated twice. Blood was collected from the inferior vena cava following sacrifice and centrifuged for 20 min at 2300g to obtain the serum. The ALT was measured using an alanine aminotransferase (ALT) activity assay kit (Colorimetric) (Cell Biolabs, Inc.) according to the manufacturer's instruction for a 96-well format.

■ ASSOCIATED CONTENT

Supporting Information

The Supporting Information is available free of charge at <https://pubs.acs.org/doi/10.1021/jacs.0c10732>.

Schemes of synthetic pathways, discussions of synthetic methods used, and figures of HPLC analysis, sensitivity of various human cancer cell lines against floxuridine, concentration-dependent anticancer activity of floxuridine and F6 prodrugs, cell viability assay, MALDI-TOF MS data, body weight changes of tumor-bearing mice after treatment, ALT levels of drug-treated mice, and ¹H, ¹³C, and ³¹P NMR spectra (PDF)

■ AUTHOR INFORMATION

Corresponding Author

Akimitsu Okamoto – Department of Chemistry and Biotechnology, Graduate School of Engineering and Research Center for Advanced Science and Technology (RCAST), The University of Tokyo, Tokyo 113-8656, Japan; orcid.org/0000-0002-7418-6237; Email: okamoto@chembio.t.u-tokyo.ac.jp

Authors

Kunihiko Morihiko – Department of Chemistry and Biotechnology, Graduate School of Engineering, The University of Tokyo, Tokyo 113-8656, Japan; orcid.org/0000-0002-9642-1031

Takuro Ishinabe – Department of Chemistry and Biotechnology, Graduate School of Engineering, The University of Tokyo, Tokyo 113-8656, Japan

Masako Takatsu – Research Center for Advanced Science and Technology (RCAST), The University of Tokyo, Tokyo 153-8904, Japan

Hiraki Osumi – Department of Chemistry and Biotechnology, Graduate School of Engineering, The University of Tokyo, Tokyo 113-8656, Japan

Tsuyoshi Osawa – Department of Chemistry and Biotechnology, Graduate School of Engineering and Research Center for Advanced Science and Technology (RCAST), The University of Tokyo, Tokyo 113-8656, Japan

Complete contact information is available at: <https://pubs.acs.org/10.1021/jacs.0c10732>

Notes

The authors declare no competing financial interest.

■ ACKNOWLEDGMENTS

This work was supported by the Tokyo Biochemical Research Foundation (TBRF) (to K.M.), the Japan Science and Technology Agency (JST) ACT-X (JPMJAX191I to K.M.), and the Japan Society for the Promotion of Science (JSPS) KAKENHI (18H03931, 18H05504, and 19K22245 to A.O.). The Table of Contents graphic was created with BioRender.com.

■ REFERENCES

- (1) Myers, C. E.; Diasio, R.; Eliot, H. M.; Chabner, B. A. Pharmacokinetics of Fluoropyrimidines - Implications for Their Clinical Use. *Cancer Treat. Rev.* **1976**, *3*, 175–183.
- (2) Grem, J. L. 5-Fluorouracil: Forty-Plus and Still Ticking. A Review of Its Preclinical and Clinical Development. *Invest. New Drugs* **2000**, *18*, 299–313.
- (3) Zhang, X.; Li, X.; You, Q.; Zhang, X. Prodrug Strategy for Cancer Cell-Specific Targeting: A Recent Overview. *Eur. J. Med. Chem.* **2017**, *139*, 542–563.
- (4) Vaupel, P.; Schlenger, K.; Knoop, C.; Höckel, M. Oxygenation of Human Tumors - Evaluation of Tissue Oxygen Distribution in Breast Cancers by Computerized O₂ Tension Measurements. *Cancer Res.* **1991**, *51* (12), 3316–3322.
- (5) Jihō, Y.; Kurihara, R.; Kawai, K.; Yamada, H.; Uto, Y.; Tanabe, K. Enzymatic Activation of Indolequinone-Substituted 5-Fluorodeoxyuridine Prodrugs in Hypoxic Cells. *Bioorg. Med. Chem. Lett.* **2019**, *29*, 1304–1307.
- (6) Liu, J.; Bu, W.; Shi, J. Chemical Design and Synthesis of Functionalized Probes for Imaging and Treating Tumor Hypoxia. *Chem. Rev.* **2017**, *117*, 6160–6224.
- (7) Lutz, S.; Liu, L.; Liu, Y. Engineering Kinases to Phosphorylate Nucleoside Analogs for Antiviral and Cancer Therapy. *Chimia* **2009**, *63*, 737–744.
- (8) Alouane, A.; Labruère, R.; Le Saux, T.; Schmidt, F.; Jullien, L. Self-Immolative Spacers: Kinetic Aspects, Structure–Property Relationships, and Applications. *Angew. Chem., Int. Ed.* **2015**, *54*, 7492–7509.
- (9) Zbaida, S.; Levine, W. G. A Novel Application of Cyclic Voltammetry for Direct Investigation of Metabolic Intermediates in Microsomal Azo Reduction. *Chem. Res. Toxicol.* **1991**, *4*, 82–88.
- (10) Sansom, G. N.; Kirk, N. S.; Guise, C. P.; Anderson, R. F.; Smaill, J. B.; Patterson, A. V.; Kelso, M. J. Prototyping Kinase Inhibitor-Cytotoxin Anticancer Mutual Prodrugs Activated by Tumour Hypoxia: A Chemical Proof of Concept Study. *Bioorg. Med. Chem. Lett.* **2019**, *29*, 1215–1219.
- (11) Zhou, F.; Fu, T.; Huang, Q.; Kuai, H.; Mo, L.; Liu, H.; Wang, Q.; Peng, Y.; Han, D.; Zhao, Z.; Fang, X.; Tan, W. Hypoxia-Activated PEGylated Conditional Aptamer/Antibody for Cancer Imaging with Improved Specificity. *J. Am. Chem. Soc.* **2019**, *141*, 18421–18427.

- (12) Yuan, P.; Zhang, H.; Qian, L.; Mao, X.; Du, S.; Yu, C.; Peng, B.; Yao, S. Q. Intracellular Delivery of Functional Native Antibodies under Hypoxic Conditions by Using a Biodegradable Silica Nanoquencher. *Angew. Chem., Int. Ed.* **2017**, *56*, 12481–12485.
- (13) Morihito, K.; Kodama, T.; Obika, S. Benzylidene Acetal Type Bridged Nucleic Acids: Changes in Properties upon Cleavage of the Bridge Triggered by External Stimuli. *Chem. - Eur. J.* **2011**, *17*, 7918–7926.
- (14) Takahashi, S.; Piao, W.; Matsumura, Y.; Komatsu, T.; Ueno, T.; Terai, T.; Kamachi, T.; Kohno, M.; Nagano, T.; Hanaoka, K. Reversible Off-On Fluorescence Probe for Hypoxia and Imaging of Hypoxia-Normoxia Cycles in Live Cells. *J. Am. Chem. Soc.* **2012**, *134*, 19588–19591.
- (15) Perche, F.; Biswas, S.; Wang, T.; Zhu, L.; Torchilin, V. P. Hypoxia-Targeted siRNA Delivery. *Angew. Chem., Int. Ed.* **2014**, *53*, 3362–3366.
- (16) Piao, W.; Hanaoka, K.; Fujisawa, T.; Takeuchi, S.; Komatsu, T.; Ueno, T.; Terai, T.; Tahara, T.; Nagano, T.; Urano, Y. Development of an Azo-Based Photosensitizer Activated under Mild Hypoxia for Photodynamic Therapy. *J. Am. Chem. Soc.* **2017**, *139*, 13713–13719.
- (17) Kiyose, K.; Hanaoka, K.; Oshiki, D.; Nakamura, T.; Kajimura, M.; Suematsu, M.; Nishimatsu, H.; Yamane, T.; Terai, T.; Hirata, Y.; Nagano, T. Hypoxia-Sensitive Fluorescent Probes for in Vivo Real-Time Fluorescence Imaging of Acute Ischemia. *J. Am. Chem. Soc.* **2010**, *132*, 15846–15848.
- (18) Piao, W.; Tsuda, S.; Tanaka, Y.; Maeda, S.; Liu, F.; Takahashi, S.; Kushida, Y.; Komatsu, T.; Ueno, T.; Terai, T.; Nakazawa, T.; Uchiyama, M.; Morokuma, K.; Nagano, T.; Hanaoka, K. Development of Azo-Based Fluorescent Probes to Detect Different Levels of Hypoxia. *Angew. Chem., Int. Ed.* **2013**, *52*, 13028–13032.
- (19) Li, Z.; Wu, M.; Bai, H.; Liu, X.; Tang, G. Light-Enhanced Hypoxia-Responsive Nanoparticles for Deep Tumor Penetration and Combined Chemo-Photodynamic Therapy. *Chem. Commun.* **2018**, *54*, 13127–13130.
- (20) Im, S.; Lee, J.; Park, D.; Park, A.; Kim, Y.; Kim, W. J. Hypoxia-Triggered Transforming Immunomodulator for Cancer Immunotherapy via Photodynamically Enhanced Antigen Presentation of Dendritic Cell. *ACS Nano* **2019**, *13*, 476–488.
- (21) Nakata, E.; Yukimachi, Y.; Kariyazono, H.; Im, S.; Abe, C.; Uto, Y.; Maezawa, H.; Hashimoto, T.; Okamoto, Y.; Hori, H. Design of a Bioreductively-Activated Fluorescent pH Probe for Tumor Hypoxia Imaging. *Bioorg. Med. Chem.* **2009**, *17*, 6952–6958.
- (22) Guise, C. P.; Abbattista, M. R.; Tipparaju, S. R.; Lambie, N. K.; Su, J.; Li, D.; Wilson, W. R.; Dachs, G. U.; Patterson, A. V. Diflavin Oxidoreductases Activate the Bioreductive Prodrug PR-104A under Hypoxia. *Mol. Pharmacol.* **2012**, *81*, 31–40.
- (23) Paine, M. J. I.; Garner, A. P.; Powell, D.; Sibbald, J.; Sales, M.; Pratt, N.; Smith, T.; Tew, D. G.; Wolf, C. R. Cloning and Characterization of a Novel Human Dual Flavin Reductase. *J. Biol. Chem.* **2000**, *275*, 1471–1478.
- (24) Garner, A. P.; Paine, M. J. I.; Rodriguez-Crespo, I.; Chinje, E. C.; De Montellano, P. O.; Stratford, I. J.; Tew, D. G.; Wolf, C. R. Nitric Oxide Synthases Catalyze the Activation of Redox Cycling and Bioreductive Anticancer Agents. *Cancer Res.* **1999**, *59* (8), 1929–1934.
- (25) Sullivan, R.; Paré, G. C.; Frederiksen, L. J.; Semenza, G. L.; Graham, C. H. Hypoxia-Induced Resistance to Anticancer Drugs Is Associated with Decreased Senescence and Requires Hypoxia-Inducible Factor-1 Activity. *Mol. Cancer Ther.* **2008**, *7*, 1961–1973.
- (26) Gmeiner, W. H.; Sahasrabudhe, P.; Pon, R. T.; Sonntag, J.; Srinivasan, S.; Iversen, P. L. Preparation of Oligomeric 2'-Deoxy-5-Fluorouridylylate of Defined Length and Backbone Composition: A Novel Pro-Drug Form of the Potent Anti-Cancer Drug 2'-Deoxy-5-Fluorouridylylate. *Nucleosides Nucleotides* **1995**, *14*, 243–253.
- (27) Gmeiner, W. H.; Debinski, W.; Milligan, C.; Caudell, D.; Pardee, T. S. The Applications of the Novel Polymeric Fluoropyrimidine F10 in Cancer Treatment: Current Evidence. *Future Oncol.* **2016**, *12*, 2009–2020.
- (28) Mou, Q.; Ma, Y.; Pan, G.; Xue, B.; Yan, D.; Zhang, C.; Zhu, X. DNA Trojan Horses: Self-Assembled Floxuridine-Containing DNA Polyhedra for Cancer Therapy. *Angew. Chem., Int. Ed.* **2017**, *56*, 12528–12532.
- (29) Jin, C.; Zhang, H.; Zou, J.; Liu, Y.; Zhang, L.; Li, F.; Wang, R.; Xuan, W.; Ye, M.; Tan, W. Floxuridine Homomeric Oligonucleotides “Hitchhike” with Albumin in Situ for Cancer Chemotherapy. *Angew. Chem., Int. Ed.* **2018**, *57*, 8994–8997.
- (30) Mou, Q.; Ma, Y.; Ding, F.; Gao, X.; Yan, D.; Zhu, X.; Zhang, C. Two-in-One Chemogene Assembled from Drug-Integrated Antisense Oligonucleotides to Reverse Chemoresistance. *J. Am. Chem. Soc.* **2019**, *141*, 6955–6966.
- (31) Zhu, L.; Guo, Y.; Qian, Q.; Yan, D.; Li, Y.; Zhu, X.; Zhang, C. Carrier-Free Delivery of Precise Drug-Chemogene Conjugates for Synergistic Treatment of Drug-Resistant Cancer. *Angew. Chem., Int. Ed.* **2020**, *59*, 17944–17950.
- (32) Gu, R.; Oweida, T.; Yingling, Y. G.; Chilkoti, A.; Zauscher, S. Enzymatic Synthesis of Nucleobase-Modified Single-Stranded DNA Offers Tunable Resistance to Nuclease Degradation. *Biomacromolecules* **2018**, *19*, 3525–3535.
- (33) Zhang, N.; Tan, C.; Cai, P.; Zhang, P.; Zhao, Y.; Jiang, Y. The Design, Synthesis and Evaluation of Hypoxia-Activated Pro-Oligonucleotides. *Chem. Commun.* **2009**, 3216–3218.
- (34) Saneyoshi, H.; Hiyoshi, Y.; Iketani, K.; Kondo, K.; Ono, A. Bioreductive Deprotection of 4-Nitrobenzyl Group on Thymine Base in Oligonucleotides for the Activation of Duplex Formation. *Bioorg. Med. Chem. Lett.* **2015**, *25*, 5632–5635.
- (35) Saneyoshi, H.; Iketani, K.; Kondo, K.; Saneyoshi, T.; Okamoto, I.; Ono, A. Synthesis and Characterization of Cell-Permeable Oligonucleotides Bearing Reduction-Activated Protecting Groups on the Internucleotide Linkages. *Bioconjugate Chem.* **2016**, *27*, 2149–2156.
- (36) Hagedorn, P.; Yakimov, V.; Ottosen, S.; Kammler, S.; Nielsen, N.; Hog, A.; Hedtjarn, M.; Meldgaard, M.; Møller, M.; Orum, H.; Koch, T.; Lindow, M. Hepatotoxic Potential of Therapeutic Oligonucleotides Can Be Predicted from Their Sequence and Modification Pattern. *Nucleic Acid Ther.* **2013**, *23* (5), 302–310.
- (37) Morihito, K.; Kasahara, Y.; Obika, S. Biological Applications of Xeno Nucleic Acids. *Mol. Biosyst.* **2017**, *13*, 235–245.